PHYSICAL REVIEW RESEARCH **6**, L032028 (2024)

Letter

Accurate and efficient Bloch-oscillation-enhanced atom interferometry

F. Fitzek [1,2,*] J.-N. Kirsten-Siemß [1,2] E. M. Rasel,[2] N. Gaaloul [2] and K. Hammerer [1,†]

[1] *Leibniz Universität Hannover, Institut für Theoretische Physik, Appelstraße 2, D-30167 Hannover, Germany*

[2] *Leibniz Universität Hannover, Institut für Quantenoptik, Welfengarten 1, D-30167 Hannover, Germany*

(Received 21 July 2023; accepted 23 May 2024; published 5 August 2024)

Bloch oscillations of atoms in optical lattices are a powerful technique that can dramatically boost the sensitivity of atom interferometers to a wide range of signals by large momentum transfer. To leverage this method to its full potential, an accurate theoretical description of losses and phases is required, going beyond existing treatments. Here, we present a comprehensive theoretical framework for Bloch-oscillation-enhanced atom interferometry and verify its accuracy through comparison with a numerical solution of the Schrödinger equation. Our approach establishes design criteria to reach the fundamental efficiency and accuracy limits of large momentum transfer using Bloch oscillations and allows us, in a broader context, to define the fundamental efficiency limit of the transport of neutral atoms using optical lattices. We compare these limits to the capabilities of current state-of-the-art experiments and make projections for the next generation of quantum sensors.

DOI: 10.1103/PhysRevResearch.6.L032028

Large-momentum-transfer (LMT) techniques are essential tools to enhance the sensitivity of atom interferometers, which are versatile quantum sensors capable of highly accurate and precise measurements with numerous applications. These include the determination of fundamental constants like the fine-structure [1,2] and gravitational constants [3], tests of general relativity [4,5], as well as applications in geophysics [6] and inertial navigation [6–9]. Bloch oscillations (BOs) of atoms in optical lattices [10,11] are a frequently utilized LMT technique in state-of-the-art experiments to generate momentum changes of 100–1000 photon recoils to either measure the fine-structure constant [1,2], hold atoms against gravity [12], or realize large spatial separations [13,14], as illustrated in Fig. 1(a). In these implementations, highly symmetric geometries or differential measurement techniques were required to suppress systematic phase uncertainties. Operating atom interferometers beyond momentum changes of 1000 photon recoils is a critical requirement for the detection of gravitational waves in the mid-frequency band and the exploration of ultralight dark matter and dark energy [15–20], as well as in advancing our understanding of the fine-structure constant measurement discrepancies [2]. For the continued progress of these fields it is essential to develop a model that accurately predicts losses and phase uncertainties for LMT sequences of BOs. So far, control of the systematic phase uncertainty is lacking due to the absence of a theory of the phase build-up during BOs.

The description of BOs is commonly based on the adiabatic theorem using instantaneous Bloch states [21,22]. Figure 1(b) illustrates an atomic wave packet localized in the fundamental Bloch band and adiabatically following the instantaneous eigenenergies for a nonvanishing lattice acceleration. The loss probability to neighboring Bloch bands at avoided crossings is calculated using the Landau-Zener (LZ) formula [22,23]. The inaccuracies of this model are well known [24–27], especially considering deep lattice depths $V_0 \gtrsim 20\, E_r$. It is, however, in this regime that one would need to operate to realize sizable LMT processes. As V_0 increases the Bloch bands become increasingly flat, which violates the applicability of the LZ formula. As we will show, the losses for a momentum transfer of 1000 photon recoils based on the widely used LZ formula differs by orders of magnitude from the numerical solution. In this article we develop a theoretical framework for BO-enhanced atom interferometers and establish design criteria for LMT Bloch pulses, reaching their fundamental efficiency limit. We use our model to confirm systematic limitations of state-of-the-art experiments and verify its accuracy through comparison with a numerical integration of Schrödinger's equation.

We consider an atom with mass m interacting with a pair of two counterpropagating light fields of adjustable intensity and frequency difference giving rise to an optical lattice with lattice constant d and wave number $k_L = \pi/d$. In a lattice-comoving reference frame, the Hamiltonian reads [23]

$$H(t) = \frac{\hat{p}^2}{2m} + V_0(t)\cos^2(k_L\hat{x}) + ma_L(t)\hat{x}. \qquad (1)$$

The lattice depth is expressed by the two-photon Rabi frequency $V_0(t) = 2\hbar\Omega(t)$. The lattice acceleration is set by the frequency difference of the light fields $a_L(t) = \frac{\pi}{k_L}\partial_t \Delta\nu(t)$ [24]. An LMT Bloch pulse consists of three separate processes, as illustrated in Fig. 1(d): First, during τ_{load} atoms

*Contact author: fitzek@iqo.uni-hannover.de

†Contact author: klemens.hammerer@itp.uni-hannover.de

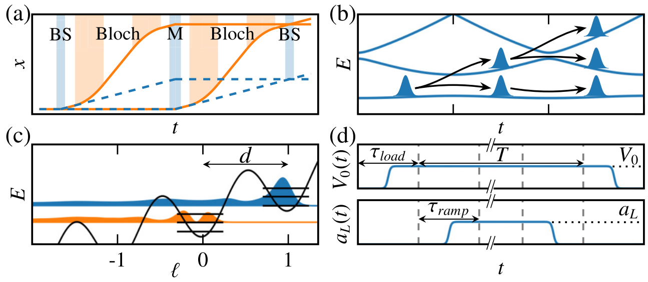

FIG. 1. (a) Space-time diagram of a Mach-Zehnder LMT atom interferometer consisting of two beam-splitter pulses (blue, BS) and one mirror pulse (blue, M). Four sequences of BOs (orange, Bloch) are used to sequentially accelerate and decelerate the arms of the interferometer. (b) Pictorial representation of LMT Bloch pulse in Bloch basis. (c) Pictorial representation of WS states $|\Psi_{\alpha=0,\,\ell=1}\rangle$ (filled blue) and $|\Psi_{\alpha=1,\,\ell=0}\rangle$ (filled orange) in tilted lattice potential [see Eq. (1)]. (d) Lattice depth $V_0(t)$ and acceleration $a_L(t)$ vs time t for an LMT Bloch pulse.

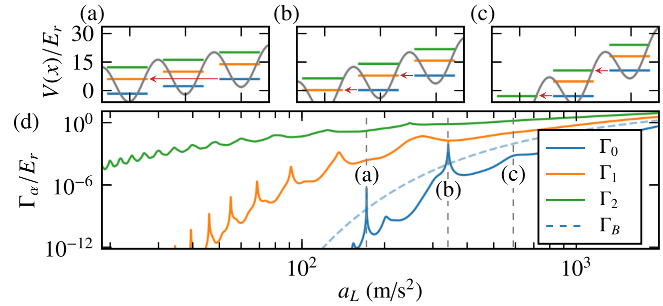

FIG. 2. (a)–(c) Tilted potential [see Eq. (1)] for accelerations indicated in (d) and a lattice depth of $V_0 = 20\,E_r$, including WS energies. Red arrows represent process of resonant tunneling between different WS ladders. (d) Linewidth of WS ladders for $V_0 = 20\,E_r$ vs peak acceleration a_L. Solid lines show linewidths for the first three WS ladders. Dashed line shows the linewidth for the fundamental WS ladder predicted by the LZ formula [23].

are adiabatically loaded into the comoving optical lattice with peak lattice depth V_0. Second, atoms and lattice undergo an acceleration phase of duration T characterized by a peak acceleration a_L and a ramping time τ_{ramp}. Finally, atoms are unloaded from the optical lattice and will have experienced a total momentum transfer of $2N\,\hbar k_L$ proportional to the number of BOs $N = T/T_B$ [28], where $T_B = 2\hbar k_L/ma_L$ denotes the Bloch period.

We base our theoretical description on so-called Wannier-Stark (WS) states $|\Psi_{\alpha,\ell}\rangle$, which are (quasi-)bound eigenstates of $H(t)$ [29,30],

$$H(t)|\Psi_{\alpha,\ell}(t)\rangle = [E_{\alpha,0}(t) + d\ell m a_L(t) - i\Gamma_\alpha(t)/2]|\Psi_{\alpha,\ell}(t)\rangle, \tag{2}$$

where ℓ denotes the lattice-site quantum number and α the quantum number labeling the so-called αth WS ladder. The eigenvalues are complex energies that depend on $V_0(t)$ and $a_L(t)$. Their imaginary part $\Gamma_\alpha(t)$ represents a linewidth for the αth WS ladder and describes tunneling losses [30]. As illustrated in Fig. 1(c), atoms that are localized in the tilted potential [see Eq. (1)] can undergo tunneling events until they escape from the optical lattice. In this case they behave like free particles represented by the infinite tail of WS states in opposite direction of motion of the optical lattice. To compute the complex WS energies in Eq. (2), a numerical routine closely related to Floquet theory is required [27,31]. We generalize this method to incorporate the treatment of adiabatic acceleration pulses, as depicted in Fig. 1(d), by developing an energy-sorting algorithm based on an analytical approximation for WS energies $E_{\alpha,l}$ [23]. Figure 2(d) displays that $\Gamma_\alpha(t)$ depends nontrivially on $a_L(t)$, exhibiting tunneling resonances [30]. In contrast, the loss rate Γ_B based on the LZ formula shows a monotonous behavior, differing dramatically from Γ_0. The position of the tunneling resonances can be explained by identifying crossings of the real part of the WS energies between different WS ladders, as shown in Figs. 2(a)–2(c). In the past, the properties and existence of the WS spectrum were controversially discussed [29,32–34], and only after decades of research efforts could a rigorous justification of the spectral properties of $H(t)$ be achieved [30]. Since then, WS states have been used to analyze experiments of cold atoms in accelerated optical lattices [11,26,27,31]. We advocate that a model based on WS states is the adequate picture to devise LMT Bloch pulses reaching their fundamental efficiency limit.

To realize optimal LMT Bloch pulses we propose adiabatic control of atoms in WS eigenstates. We first focus on the dynamics under the adiabatic approximation. Figure 2(d) demonstrates that due to the generally narrower linewidth, it is advantageous to drive LMT Bloch pulses in the fundamental WS ladder [35]. This observation holds for arbitrary lattice depths [23] and has direct implications for the process of loading atoms into the optical lattice, which we infer from the properties of WS states for vanishing accelerations. In this limit we make use of the single-band approximation and neglect hopping processes to neighboring lattice sites, resulting in $|\Psi_{\alpha,\ell}\rangle|_{a_L=0} = |w_{\alpha,\ell}\rangle$, where $|w_{\alpha,\ell}\rangle$ are Wannier states of the Bloch band α localized at lattice site ℓ. Consequently, only atoms loaded into the fundamental Bloch band serve as a suitable initial condition for the acceleration phase to minimize tunneling losses. This is achieved for an atomic momentum distribution $\varphi(p)$ that vanishes outside the Brillouin zone $[-\hbar k_L, \hbar k_L]$ and sufficiently long loading times τ_{load}, as is common in state-of-the-art experiments [1,2,12–14]. If these requirements are violated, atoms will populate excited WS ladders and experience increased tunneling losses, as seen in Fig. 2(d). We apply the adiabatic approximation during τ_{load} and find $|\psi(\tau_{\mathrm{load}})\rangle = \sum_\ell g_\ell |w_{0,\ell}\rangle$ with

$$g_\ell = \int_{-\hbar k_L}^{\hbar k_L} \mathrm{d}p\, \varphi(p)\, e^{-i\int_0^{\tau_{\mathrm{load}}} \mathrm{d}t'\, E_0[V_0(t'),\, p]/\hbar} e^{ipd\ell/\hbar}, \tag{3}$$

where $E_0(V_0, p)$ are Bloch eigenenergies of $H(t)$ for vanishing acceleration with a fixed lattice depth V_0 and quasimomentum $p \in [-\hbar k_L, \hbar k_L]$. Based on Eq. (2), we apply the adiabatic approximation during the time T for Hamiltonians with a discrete and nondegenerate complex spectrum [36–38]. As long as there exists a finite complex energy gap between the fundamental and excited WS states and for sufficiently small

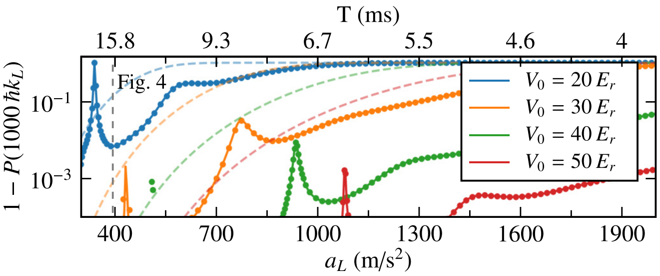

FIG. 3. Losses for an adiabatic $1000\,\hbar k_L$ LMT Bloch pulse vs peak acceleration a_L for a given lattice depth V_0 and ramping time of $\tau_{\mathrm{ramp}} = 1$ ms. The upper axis shows the corresponding acceleration time T [see Fig. 1(b)]. Solid lines represent losses based on the WS model [see Eq. (4)]. Dots show the numerical solution. Dashed lines show the predicted losses based on the LZ formula [23].

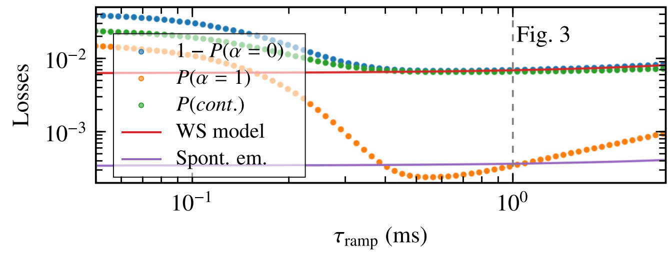

FIG. 4. Losses for a $1000\,\hbar k_L$ LMT Bloch pulse vs acceleration ramp time τ_{ramp} for a peak lattice depth of $V_0 = 20\,E_r$. Red solid line represents losses based on the WS model. Dots show the results of numerical solutions, distinguishing between total losses from the WS ladder $\alpha = 0$ (blue dots), losses to the WS ladder $\alpha = 1$ (orange dots), and tunneling losses (green dots). Solid purple line shows spontaneous emission losses [23]. The peak acceleration is optimally chosen at $a_L = 393.5$ m/s^2, as determined from Fig. 3.

changes of $a_L(t)$, we write

$$|\psi(t)\rangle = \sum_{\ell} e^{-i\int_0^t \mathrm{d}t' E_{0,0}(t')/\hbar} e^{-id\ell p_L(t)/\hbar} \times e^{-\int_0^t \mathrm{d}t' \Gamma_0(t')/2\hbar}\, g_\ell |\Psi_{0,\ell}(t)\rangle, \tag{4}$$

where the time-dependent WS eigenvalue $E_{0,0}(t') - i\Gamma_0(t')/2$ is defined in Eq. (2) and the velocity of the optical lattice as $p_L(t)/m = \int_0^t \mathrm{d}t' a_L(t')$. Equation (4) describes phases and losses of the atomic wave packet with a momentum distribution $\varphi(p)$ undergoing an adiabatic LMT Bloch pulse.

The finite lifetime of WS states has important implications when designing LMT Bloch pulses. Figure 3 shows that for adiabatic LMT Bloch pulses the fundamental and dominant loss mechanism is given by tunneling losses. This is demonstrated by the excellent agreement between the adiabatic WS model in Eq. (4) and a numerical solution, where we solve Schrödinger's equation for the Hamiltonian in Eq. (1) using the split-step Fourier method [39,40]. We identify combinations of optimal lattice depths and accelerations to minimize losses for LMT Bloch pulses. They are directly connected to Γ_0 and the occurrence of resonant tunneling. In contrast, the losses predicted by the LZ formula [21,22] deviate dramatically from the numerical solution for the entire range of parameters shown.

We proceed to discuss nonadiabatic deviations from the predictions of Eq. (4). At tunneling resonances the complex energy gap can become very small and hence the tunneling probability from the fundamental to excited WS ladders increases when passing through them, leading to nonadiabatic losses. Once atoms are localized in an excited WS ladder, they are subject to increased tunneling losses quantified by Γ_α, as shown in Fig. 2(d), resulting in reduced fidelities. Atoms that remain in excited WS ladders until $a_L(t)$ is turned off are localized in excited Bloch bands, as evident from $|\Psi_{\alpha,\ell}\rangle|_{a_L=0} = |w_{\alpha,\ell}\rangle$. During the adiabatic unloading from the optical lattice, these atoms are mapped to momenta that differ, depending on the band number α, by multiples of $\pm 2\,\hbar k_L$ from the target momentum $2N\,\hbar k_L$. For constant accelerations the Hamiltonian $H(t) \equiv H$ in Eq. (1) will be time-independent and nonadiabatic losses cannot occur. The adiabaticity of an LMT Bloch pulse can be controlled by adjusting the acceleration ramp time τ_{ramp} [41]. In Fig. 4 we numerically analyze tunneling and nonadiabatic losses for a $1000\,\hbar k_L$ LMT Bloch pulse. For small times τ_{ramp}, the flat-top pulse, as depicted in Fig. 1(d), resembles a box pulse causing a large fraction of atoms to tunnel to excited WS ladders. This results in an increased amount of tunneling losses with contributions from all WS ladders that were populated during the pulse, as shown in Fig. 4. For larger times τ_{ramp} nonadiabatic tunneling to excited WS ladders is significantly reduced and the total losses can be accurately computed using Eq. (4). For increasingly larger times τ_{ramp} we observe a slight increase of nonadiabatic excitations due to the prolonged time atoms spend at tunneling resonances. This gives rise to an optimal acceleration ramp time τ_{ramp} with minimal losses, accurately determined by Eq. (4).

Moreover, our model establishes a general result for neutral atom transport via optical lattices. Since the generic WS spectrum in Eq. (2) obeys the property $\Gamma_0 \leqslant \Gamma_{\alpha>0}$, the fundamental efficiency limit for a generalized LMT Bloch pulse, defined by arbitrary lattice depth and acceleration ramps, is determined by tunneling losses of the fundamental WS ladder $P_{\mathrm{fundamental}} = e^{-\int_0^t \mathrm{d}t'\, \Gamma_0[V_0(t'),a_L(t')]/\hbar}$. This limit equally applies to nonadiabatic transport schemes that are, for instance, proposed by quantum optimal control theory [42–47].

Apart from tunneling and nonadiabatic losses, atoms will also experience losses due to spontaneous emission. We estimate this additional loss channel based on a laser system used in a state-of-the-art experiment [13] for an optimal LMT Bloch pulse with minimal losses at peak lattice depth $V_0 = 20\,E_r$ and peak acceleration $a_L = 393.5$ m/s^2, as determined from Fig. 3. In this setting losses due to spontaneous emission are three times larger than tunneling losses [23], highlighting the need for more powerful laser systems to operate efficient LMT Bloch pulses. However, considering a recently developed laser system for atom interferometry [48] losses due to spontaneous emission are orders of magnitude smaller than tunneling losses for moderate lattice depths $V_0 \lesssim 35\,E_r$ [23], as shown in Fig. 4 for $V_0 = 20\,E_r$.

The excellent agreement between the WS model and the numerical solution enables us to accurately quantify systematic errors connected to adiabatic LMT Bloch pulses used in atom interferometers [49]. A relevant contribution to the overall phase variance is induced by intensity fluctuations of

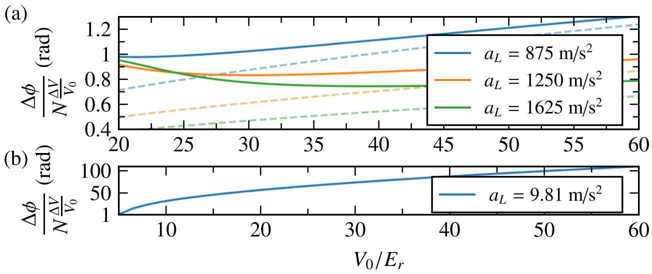

FIG. 5. Phase uncertainty induced by lattice-depth fluctuations vs peak lattice depth V_0 for different peak accelerations a_L. Solid lines represent the phase uncertainty based on the WS model, dashed lines show the phase uncertainty evaluated with the adiabatic Bloch model [23] for (a) exemplary peak accelerations that allow for high-fidelity LMT Bloch pulses, as determined in Fig. 3, and (b) the local gravitational acceleration.

the light pulse. Based on our model, the phase accrued in an adiabatic $2N\hbar k_L$ Bloch pulse in a single interferometer arm is given by $\phi = E_{0,0}NT_B/\hbar$; cf. Eq. (4). A relative fluctuation ΔV in lattice depth between two arms in Fig. 1(a) will therefore induce a variation of the relative phase

$$\frac{\Delta\phi}{N\,\dfrac{\Delta V}{V_0}} = 2\pi\left|\frac{\partial E_{0,0}}{\partial V_0}\right|\frac{V_0}{dma_L}. \tag{5}$$

Here, we refer the phase fluctuation to the number of BOs N and the relative lattice-depth fluctuation $\Delta V/V_0$. In Figs. 5(a) and 5(b) we show phase changes for exemplary accelerations that allow for high-fidelity LMT Bloch pulses. We observe a general tendency towards larger phase uncertainties using smaller accelerations due to the prolonged time atoms spend in the optical lattice; cf. Eq. (5). Based on Fig. 5(a), we consider the requirements to achieve a phase uncertainty of $\Delta\phi = 1$ mrad. We find that the level of relative intensity stabilization needed in this case is $\Delta V/V_0 \simeq 10^{-6}$. This presents a significant challenge in utilizing LMT Bloch pulses in atom interferometers and highlights the advantage of symmetric atom interferometer geometries in alleviating the detrimental effects of relative intensity fluctuations [13,14].

We use our model to explain the performance limitations of three different state-of-the-art experiments [2,12,17] due to ΔV, which originates from a variance in the tilt angle $\Delta\theta$ of the beam axis, causing transversal displacements of the atomic clouds. First, we analyze the fine-structure constant measurement presented in Morel *et al.* [2,50]. This setup utilizes a Ramsey-Bordé geometry with ^{87}Rb atoms, where both interferometer arms are accelerated simultaneously with a momentum transfer of $1000\,\hbar k_L$. For small $\Delta\theta$ and a given separation between the interferometer arms z, this results in $\Delta V/V_0 = \Delta\theta^2 z^2/2w_0^2$, using the harmonic approximation for the Gaussian laser mode with waist w_0. To reach a relative uncertainty in h/m at the level of 10^{-9} in one shot, four central fringes need to be resolved with a phase uncertainty of $\Delta\phi = 1$ mrad, as reported in [50]. Using our model, we provide an upper bound for the relative intensity stabilization at $\Delta V/V_0 \lesssim 1.51 \times 10^{-6}$ which is equivalent to a maximal variance of the tilt angle of $\Delta\theta \lesssim 16.5$ mrad. To improve the precision by one order of magnitude, the variance needs to be bound by $\Delta\theta \lesssim 5.2$ mrad.

As a second example, we analyze the cavity experiment presented in Panda *et al.* [12]. In this setup, a spatially separated superposition of ^{133}Cs atoms is adiabatically loaded into a vertically aligned optical lattice and held against gravity; cf. Fig. 5(b). The record-breaking coherence time of 1 minute corresponds to $N \approx 92\,435$ BOs. Again, oscillatory tilts of the vertical cavity axis cause a relative lattice-depth instability between the atomic clouds of $\Delta V/V_0 \simeq \Delta\theta z/w_0$ in the case of a shallow optical lattice with $V_0 = 7\,E_r$ [12]. These oscillatory tilts lead to a loss of contrast, which are explained in [12] using semiclassical Monte Carlo simulations that model the transversal motion of atoms in the Gaussian beam. Alternatively, we infer from Eq. (5) of our one-dimensional model a phase uncertainty of $\Delta\phi \approx 0.9$ rad for a holding time of 1 minute and a tilt uncertainty of $\Delta\theta = 300$ µrad [12]. This is consistent with the loss of contrast observed in the experiment. The temperature dependency of the observed contrast decay [12] could be treated in our description by extending to a cylindrically symmetric description of the Gaussian beam.

As a third example, we analyze a proposal for gravitational wave detection using atom interferometers presented in Canuel *et al.* [17,51]. The targeted baseline design foresees a double-loop geometry, including LMT beam splitters based on Bragg diffraction [52,53] and BOs with $N = 500$ and a phase resolution of $\Delta\phi = 1$ µrad. An optimal combination of lattice depth and acceleration for LMT Bloch pulses can be determined with the help of the WS model, as presented in Fig. 3. For exemplary lattice depths and accelerations based on Fig. 5(a) we quantify the necessary relative intensity stabilization between the two atomic trajectories in each interferometry arm to the level of $\Delta V/V_0 \approx 10^{-9}$. This result highlights the stringent requirements necessary for gravitational wave detection using LMT atom interferometers.

In summary, we have developed a model to design and evaluate BO-enhanced atom interferometers, providing insights into the fundamental loss processes and quantifying systematic errors. More generally, we defined the fundamental efficiency limit of neutral atom transport using optical lattices. Using our framework, we show that there exist optimal combinations of ramping times, peak lattice depths, and accelerations to drive high-fidelity LMT Bloch pulses. To verify these predictions, we compare with numerical solutions of Schrödinger's equation. Our theoretical description provides the basis for considering other relevant systematic errors, such as phase noise or residual vibrations. Furthermore, we can consider the influence of spontaneous emission, including the analysis of transversal effects [54,55]. In this context, our theoretical work presented in this article is the foundational piece for a comprehensive theoretical framework of LMT Bloch pulses for high-accuracy and high-precision atom interferometers.

Note added. Recently, we discussed with the group of S. Gupta, University of Washington, Seattle, recent related experimental work [56]. We present a comprehensive discussion and explanation of their results using the WS model in Eq. (4) in the Supplemental Material [23]. The results presented here were achieved by computations carried out on the cluster system at the Leibniz University of Hannover, Germany.

This work was funded by the Deutsche Forschungsgemeinschaft (German Research Foundation) under Germany's Excellence Strategy (EXC-2123 QuantumFrontiers Grant No. 390837967) and through CRC 1227 (DQ-mat) within Projects No. A05, No. B07, as well as No. B09, and the German Space Agency (DLR) with funds provided by the Federal Ministry for Economic Affairs and Climate Action due to an enactment of the German Bundestag under Grants No. 50WM2450A (QUANTUS-VI), No. 50WM2245A (CAL-II), No. 50WM2263A (CARIOQA-GE), No. 50WM2253A (AI-Quadrat), No. 50NA1957 (QGYRO), and No. 50NA2106 (QGYRO+). We acknowledge funding by the SQUEIS project – grant No. 499225223 – within the QuantERA II Programme and by the AGAPES project – grant No. 530096754 within the ANR-DFG 2023 Programme. J.-N. K.-S. acknowledges support from QuantumFrontiers through the QuantumFrontiers Entrepreneur Excellence Programme (QuEEP).

[1] R. H. Parker, C. Yu, W. Zhong, B. Estey, and H. Müller, Measurement of the fine-structure constant as a test of the Standard Model, Science **360**, 191 (2018).

[2] L. Morel, Z. Yao, P. Cladé, and S. Guellati-Khélifa, Determination of the fine-structure constant with an accuracy of 81 parts per trillion, Nature (London) **588**, 61 (2020).

[3] G. Rosi, F. Sorrentino, L. Cacciapuoti, M. Prevedelli, and G. M. Tino, Precision measurement of the Newtonian gravitational constant using cold atoms, Nature (London) **510**, 518 (2014).

[4] S. Dimopoulos, P. W. Graham, J. M. Hogan, and M. A. Kasevich, General relativistic effects in atom interferometry, Phys. Rev. D **78**, 042003 (2008).

[5] P. Asenbaum, C. Overstreet, M. Kim, J. Curti, and M. A. Kasevich, Atom-interferometric test of the equivalence principle at the 10^{-12} level, Phys. Rev. Lett. **125**, 191101 (2020).

[6] K. Bongs, M. Holynski, J. Vovrosh, P. Bouyer, G. Condon, E. Rasel, C. Schubert, W. P. Schleich, and A. Roura, Taking atom interferometric quantum sensors from the laboratory to real-world applications, Nat. Rev. Phys. **1**, 731 (2019).

[7] R. Geiger *et al.*, Detecting inertial effects with airborne matter-wave interferometry, Nat. Commun. **2**, 474 (2011).

[8] P. Cheiney, L. Fouché, S. Templier, F. Napolitano, B. Battelier, P. Bouyer, and B. Barrett, Navigation-compatible hybrid quantum accelerometer using a Kalman filter, Phys. Rev. Appl. **10**, 034030 (2018).

[9] R. Geiger, A. Landragin, S. Merlet, and F. Pereira Dos Santos, High-accuracy inertial measurements with cold-atom sensors, AVS Quantum Sc. **2**, 024702 (2020).

[10] M. Ben Dahan, E. Peik, J. Reichel, Y. Castin, and C. Salomon, Bloch oscillations of atoms in an optical potential, Phys. Rev. Lett. **76**, 4508 (1996).

[11] S. R. Wilkinson, C. F. Bharucha, K. W. Madison, Q. Niu, and M. G. Raizen, Observation of atomic Wannier-Stark ladders in an accelerating optical potential, Phys. Rev. Lett. **76**, 4512 (1996).

[12] C. D. Panda, M. Tao, J. Egelhoff, M. Ceja, V. Xu, and H. Müller, Coherence limits in lattice atom interferometry at the one-minute scale, Nat. Phys. (2024), doi:10.1038/s41567-024-02518-9.

[13] M. Gebbe *et al.*, Twin-lattice atom interferometry, Nat. Commun. **12**, 2544 (2021).

[14] Z. Pagel, W. Zhong, R. H. Parker, C. T. Olund, N. Y. Yao, and H. Müller, Symmetric Bloch oscillations of matter waves, Phys. Rev. A **102**, 053312 (2020).

[15] P. W. Graham, J. M. Hogan, M. A. Kasevich, and S. Rajendran, New method for gravitational wave detection with atomic sensors, Phys. Rev. Lett. **110**, 171102 (2013).

[16] B. Canuel, A. Bertoldi, L. Amand *et al.*, Exploring gravity with the MIGA large scale atom interferometer, Sci. Rep. **8**, 14064 (2018).

[17] B. Canuel *et al.*, ELGAR—a European laboratory for gravitation and atom-interferometric research, Classical Quantum Gravity **37**, 225017 (2020).

[18] M.-S. Zhan *et al.*, ZAIGA: Zhaoshan long-baseline atom interferometer gravitation antenna, Int. J. Mod. Phys. D **29**, 1940005 (2020).

[19] L. Badurina *et al.*, AION: An atom interferometer observatory and network, J. Cosmol. Astropart. Phys. 05 (2020) 011.

[20] M. Abe *et al.*, Matter-wave atomic gradiometer interferometric sensor (MAGIS-100), Quantum Sci. Technol. **6**, 044003 (2021).

[21] F. Bloch, Über die Quantenmechanik der Elektronen in Kristallgittern, Z. Phys. **52**, 555 (1929).

[22] C. Zener, A theory of the electrical breakdown of solid dielectrics, Proc. R. Soc. Lond. A **145**, 523 (1934).

[23] See Supplemental Material at http://link.aps.org/supplemental/10.1103/PhysRevResearch.6.L032028 for additional information concerning the discussion of LMT Bloch pulses and the WS model as developed in the main article. We first summarize the application of the widely-used description of LMT Bloch pulses using instantaneous Bloch states. Second, we provide a rigorous definition and construction of WS states and describe a numerical algorithm to compute the complex WS spectrum, including the case of arbitrarily small lattice accelerations. Next, we connect the WS model to relevant topics in the field of quantum sensing and atom interferometry such as the influence of spontaneous emission and the occurrence nonadiabatic losses.

[24] E. Peik, M. Ben Dahan, I. Bouchoule, Y. Castin, and C. Salomon, Bloch oscillations of atoms, adiabatic rapid passage, and monokinetic atomic beams, Phys. Rev. A **55**, 2989 (1997).

[25] M. Holthaus, Bloch oscillations and Zener breakdown in an optical lattice, J. Opt. B: Quantum Semiclassical Opt. **2**, 589 (2000).

[26] C. Sias, A. Zenesini, H. Lignier, S. Wimberger, D. Ciampini, O. Morsch, and E. Arimondo, Resonantly enhanced tunneling of Bose-Einstein condensates in periodic potentials, Phys. Rev. Lett. **98**, 120403 (2007).

[27] P. Cladé, M. Andia, and S. Guellati-Khélifa, Improving efficiency of Bloch oscillations in the tight-binding limit, Phys. Rev. A **95**, 063604 (2017).

[28] For nonvanishing τ_{ramp}, T is determined by integrating $a_L(t)$ and solving for the final velocity $2N\hbar k_L/m$.

[29] G. H. Wannier, Wave functions and effective Hamiltonian for Bloch electrons in an electric field, Phys. Rev. **117**, 432 (1960).
[30] G. Nenciu, Dynamics of band electrons in electric and magnetic fields: Rigorous justification of the effective Hamiltonians, Rev. Mod. Phys. **63**, 91 (1991).
[31] M. Glück, A. R. Kolovsky, and H. J. Korsch, Wannier–Stark resonances in optical and semiconductor superlattices, Phys. Rep. **366**, 103 (2002).
[32] J. Zak, Stark Ladder in solids? Phys. Rev. Lett. **20**, 1477 (1968).
[33] G. H. Wannier, Stark Ladder in solids? A reply, Phys. Rev. **181**, 1364 (1969).
[34] J. Zak, Stark Ladder in solids? A reply to a reply, Phys. Rev. **181**, 1366 (1969).
[35] We discuss excited-band Bloch oscillations proposed by [57] in [23].
[36] A. Mondragón and E. Hernández, Berry phase of a resonant state, J. Phys. A: Math. Gen. **29**, 2567 (1996).
[37] F. Keck, H. J. Korsch, and S. Mossmann, Unfolding a diabolic point: A generalized crossing scenario, J. Phys. A: Math. Gen. **36**, 2125 (2003).
[38] S. Ibáñez and J. G. Muga, Adiabaticity condition for non-Hermitian Hamiltonians, Phys. Rev. A **89**, 033403 (2014).
[39] M. D. Feit, J. A. Fleck, and A. Steiger, Solution of the Schrödinger equation by a spectral method, J. Comput. Phys. **47**, 412 (1982).
[40] F. Fitzek, J.-N. Siemß, S. Seckmeyer, H. Ahlers, E. M. Rasel, K. Hammerer, and N. Gaaloul, Universal atom interferometer simulation of elastic scattering processes, Sci. Rep. **10**, 22120 (2020).
[41] We discuss the lattice-shift method proposed by [27] in [23].
[42] C. Brif, R. Chakrabarti, and H. Rabitz, Control of quantum phenomena: Past, present and future, New J. Phys. **12**, 075008 (2010).
[43] G. E. Karniadakis, I. G. Kevrekidis, L. Lu, P. Perdikaris, S. Wang, and L. Yang, Physics-informed machine learning, Nat. Rev. Phys. **3**, 422 (2021).
[44] M. H. Goerz, M. A. Kasevich, and V. S. Malinovsky, Robust optimized pulse schemes for atomic fountain interferometry, Atoms **11**, 36 (2023).
[45] J. C. Saywell *et al.*, Enhancing the sensitivity of atom-interferometric inertial sensors using robust control, Nat. Commun. **14**, 7626 (2023).
[46] G. Louie, Z. Chen, T. Deshpande, and T. Kovachy, Robust atom optics for Bragg atom interferometry, New J. Phys. **25**, 083017 (2023).
[47] Z. Chen, G. Louie, Y. Wang, T. Deshpande, and T. Kovachy, Enhancing strontium clock atom interferometry using quantum optimal control, Phys. Rev. A **107**, 063302 (2023).
[48] M. Kim, R. Notermans, C. Overstreet, J. Curti, P. Asenbaum, and M. A. Kasevich, 40 W, 780 nm laser system with compensated dual beam splitters for atom interferometry, Opt. Lett. **45**, 6555 (2020).
[49] We present a comparison of the phase evolution between the WS model in Eq. (4) and a corresponding numerical solution in [23].
[50] L. Morel, High sensitivity matter-wave interferometry: Towards a determination of the fine structure constant below 10-10, Ph.D. thesis, Sorbonne Université, 2019.
[51] B. Canuel *et al.*, Technologies for the ELGAR large scale atom interferometer array, arXiv:2007.04014.
[52] P. J. Martin, B. G. Oldaker, A. H. Miklich, and D. E. Pritchard, Bragg scattering of atoms from a standing light wave, Phys. Rev. Lett. **60**, 515 (1988).
[53] D. M. Giltner, R. W. McGowan, and S. A. Lee, Theoretical and experimental study of the Bragg scattering of atoms from a standing light wave, Phys. Rev. A **52**, 3966 (1995).
[54] H. Pichler, A. J. Daley, and P. Zoller, Nonequilibrium dynamics of bosonic atoms in optical lattices: Decoherence of many-body states due to spontaneous emission, Phys. Rev. A **82**, 063605 (2010).
[55] M. Glück, F. Keck, A. R. Kolovsky, and H. J. Korsch, Wannier-Stark states of a quantum particle in 2D lattices, Phys. Rev. Lett. **86**, 3116 (2001).
[56] T. Rahman, A. Wirth-Singh, A. Ivanov, D. Gochnauer, E. Hough, and S. Gupta, Bloch oscillation phases investigated by multipath Stückelberg atom interferometry, Phys. Rev. Res. **6**, L022012 (2024).
[57] K. E. McAlpine, D. Gochnauer, and S. Gupta, Excited-band Bloch oscillations for precision atom interferometry, Phys. Rev. A **101**, 023614 (2020).